Collision Risk Assessment between UAS and Landing Aircraft in Restricted Airspace near Airports using 3D Monte-Carlo Simulation

C.H. John Wang,* Shi Kun Tan,†
Air Traffic Management Research Institute, Nanyang Technological University, Singapore

and
Kin Huat Low ‡
School of Mechanical and Aerospace Engineering, Nanyang Technological University, Singapore

The availability of off the shelf, easy to control, unmanned aerial systems (UAS) on the market has led to an increase in report of UAS incursion into aerodrome. Such incursions would often result in lengthy airport shutdowns and cause disruption to air traffic operations throughout the region. Additionally, advancement in UAS flight control, motor efficiency, and battery life made the UAS more attractive to cargo operators for carrying parcels, both in urban area and near major port of call. While advancements have been made in the past decade in detection and avoidance of UAS traffics, the systems depend on either having fully cooperative traffic or sensor capability beyond what is currently available. This paper presents a 3D collision risk assessment model that was created to assess both the collision risk posed by an intruding non-cooperative UAS, as well as the safety risk associated with UAS operating within the 5km restricted airspace using predetermined route. Monte-Carlo simulations based on the 3D flight dynamics of the UAS are used to calculate the probability of collision at each time-step under the different scenarios.

I. Introduction

The rapid development of recreational multi-copter in recent years has made the unmanned aerial systems (UAS) more accessible to the general population. The advancement in flight computers also meant that UAS operators does not need to go through training to operate these vehicles. This results in a large number of inexperienced UAS operators flying the UAS with little to no knowledge of the associated aviation regulations and lead to a raising number incidents of UAS intrusion into restricted airspace has been reported. To prevent the safety hazard of UAS collision with manned aircraft operating in the same airspace, airport could be shut down for as much as a few hours, as seen in recent incidents [1–3]. While technologies such as geofencing were developed to prevent such incursion, its function is dependent on the UAS knowing its position relative to the restricted airspace. As most UAS available on the market are not equipped with transponders the broadcast its position, the UAS would need to be treated as non-cooperative traffic by the air traffic controllers.

The recent advancement in technologies associated with UAS flight performance, such as improved motor efficiency and battery capacity, has made the UAS a more attractive platform for delivery companies and warehouses. Several companies, such as Amazon Inc., are exploring the use of UAS for parcel delivery as well as moving goods between storage locations. In time, it could become possible to use UAS to transfer parcels from the cargo terminal of the delivery company directly to the customer's doorstep. For that to happen, though, a method would need to be developed to assess the collision risk associated with each of the UAS's flight plans when operating in close proximity to commercial flight corridors.

This paper presents a 3D collision risk assessment model that was created to assess the collision risk posed by an intruding non-cooperative UAS into the 5km restricted airspace surrounding the Singapore airports [4] (referred to as "restricted airspace" below), which could then be used to create the three dimensional alert zones that could be used by the air traffic controllers (ATC). The alert zone setup could help the ATC to quickly evaluate the threat posed by

*Research Fellow, AIAA Member
†Project Officer
‡Professor, AIAA Member

the UAS and decide the immediate actions that needs to be taken; it could also be used to identify the portion of the restricted airspace that needs enhanced monitoring for UAS incursion. This is accomplished by using Monte-Carlo simulation based on the flight characteristics of the UAS to predict the UAS position distribution for each time-step as described in Section III.

II. Literature Review

Collision prevention in airspace is generally handled by the air traffic controllers (ATC) well in advance of a possible conflict through the usage of primary radar or the secondary surveillance radar, which collects ADS-B transponder data with an update rate of no greater than 3 seconds [5]. In the rare cases where the ATC did not notice the aircraft pair getting too close to each other, the Airborne Collision Avoidance System (ACAS) would acts as a fail-safe to prevent a possible collision. The ACAS accomplishes this by utilizing a specialized transponder that identifies other ACAS equipped aircraft that is on a collision course at 1 second interval; the system then provides a warning to the pilots on the incoming traffic and would issue a resolution advisory if no corrective action was taken after a period of time [6]. The transponder systems, broadcasting the position and velocity of the aircraft every few seconds, allowed the ACAS equipment to quickly detect possible conflict and generate the necessary action for its resolution. However, such constant flow of data will not be available for non-cooperative intruders without ground-based primary sensors installed.

Ground-based detection of intruding UAS could be accomplished using a number of active and passive detection technologies. Active detection of UAS is generally achieved using Pulse-Doppler radar, while the passive detection technologies utilize receivers to capture the energy reflection/emission from the UAS, e.g. camera for visible/IR light reflections, radio spectrum sensor for controller transmissions, or acoustic sensor for noise emissions. Some of the detection methods are more susceptible to environmental conditions or ambient noise than others, such as camera under low visibility conditions or acoustic sensor in high traffic area, thus limiting its effective detection range. Of the eight systems surveyed in a 2016 Massachusetts Department of Transportation review [7], only four of those were capable of covering the 5km restricted airspace surrounding the runway. The four systems with sufficient range utilizes either Doppler-radar technology or radio-frequency (RF) spectrum sensor.

Without the UAS detecting equipment, the information available to the air traffic controller on the non-cooperative intruding UAS in restricted airspace can be very limited. It might consist of only the estimated flight performance of the UAS (based on the type of UAS e.g. recreational UAS or payload capable commercial UAS) and the position of its initial incursion from sighting reports. Based on the reported initial conditions, the collision risk assessment could be calculated either based on the estimated closest point of approach (CPA) a la the ACAS system [6] or the collision prevention system used in UAS traffic avoidance algorithm [8, 9]. However, the margin of error in UAS collision forecast is expected to be quite high due to uncertainties in the initial position and estimated flight performance of the UAS. The margin of error could be reduced through the availability of tracking sensors.

In a way, the modeling of the collision risk could be viewed as an instantaneous snapshot of the UAS detect-and-avoid (DAA) research [8], which is rooted in the research done for the airborne collision avoidance system (ACAS) developed for civil aviation traffic [10]. In general, airborne traffic collision avoidance includes the following components: detection of traffic, propagation of states, detection of conflict, and resolution of the conflict [11]. In this study, the detection of traffic would depends on the availability, or the lacking, of UAS tracking sensors, while the simulation tool performs the propagation of states, i.e. path prediction, and detection of conflict. The resolution of conflict is not in the scope of this study.

Predicting the range of possible future position of the aircraft is generally conducted through three different methods in ACAS related research: the nominal (intention) based prediction, the worst-case (maximum range) based prediction, and the probabilistic based prediction [10, 11]. The nominal method assesses the collision risk by extrapolating the aircraft trajectories of both the host and the incoming traffic by maintaining the current velocity and direction of the two aircraft; the worst-case method predicts collision by evaluating the possible intersection of the volume of motions of the two aircraft, which is defined by their maximum range of motion; the probabilistic method is further split into three types: predicting the trajectory by supplementing the deterministic aircraft trajectory with probability distribution function [12–14]; by tallying results from Monte Carlo simulation using aircraft performance information and known initial position [10]; or by a combination of both by continuously updating the initial conditions for the Monte-Carlo simulation as new sensor data becomes available [9, 15].

For a prediction system based on the ACAS framework, the prediction of possible collision is calculated using the closest point of approach (CPA) between the predicted trajectories of the two aircraft in question [6]. In the case where probabilistic path prediction was used, the collision chance is assessed by calculating the overlap between the

probable spatial distribution of the UAS and the alert regions surrounding the aircraft [10]. In the case where no tracking information is available on the intruding UAS, path prediction would not be possible using the nominal method and the deterministic approach. The usage of maximum UAS reach was also ruled out due to high maneuverability of the multi-copter system and the lack of provision for navigational error either due to difference in air density along the way, minor adjustments by operators to stay on the perceived course, or power imbalance in flight control circuit that introduced minor imbalance in thrust. The UAS path prediction would thus be implemented using the Monte-Carlo simulation.

Following the prediction of the distribution of possible UAS future positions using Monte-Carlo simulation, the risk of collision could be predicted by counting the number of Monte-Carlo samples that fall within the protected volume surrounding the aircraft [10]. Depending on the location, the expected traffic type, and the level of damage that could be inflicted, the protected volumes surrounding the aircraft could be either a partial cylinder covering only the frontal area of the aircraft (as in the case of bird strike) [16], or a full cylinder with a pre-defined "safe" radius and height [9, 14]. The later, full cylindrical, approach is based on the protected volume defined for the TCAS II/ACAS II framework [6].

III. Methodology

Two different conflict scenarios will be considered in this study, depending on the available information about the UAS and its intention. The first is for a non-cooperative intruding UAS with unknown intention, and the second for a cooperative UAS working inside the restricted airspace, e.g. along a path under the flight corridor, with known flight plan. An intersecting path from the position of the UAS towards the flight corridor, i.e. under the assumption of worst-case intention, would be created for the first case, while the path towards the next waypoint would be used for the second.

The total simulation time for each conflict prediction case would be limited to 70 seconds, which is based on the time required for an aircraft to cross the 5km distance at 140 knots. While longer simulation time is possible, the spatial distribution of the samples would be more dispersed; the probability of external factors, unaccounted for at the start of the simulation, appearing would also be higher.

Modifications were made to the 2D Monte-Carlo UAS path prediction code used in the previous investigation [17] to account for the changes in flight dynamics needed to accomplish the change in UAS elevation. While the change in acceleration is still assumed to be zero during each time step, the calculation of the UAS's thrust, drag, and attitude is no longer explicit. The changes made to the code that determines the equation of motion for the UAS are presented in Section III.A.

A major consideration when performing 3D collision prediction in terminal airspace is the protected volume that surrounds the commercial aircraft operating there. Unlike the 2D collision prediction case, the TCAS protected volume (PV) could no longer be used. This is because the PV defined under ACAS II extends to 850 ft above and below the reported altitude of the commercial aircraft, making it impossible for an UAS to cross below the flight corridor without intruding into PV. Section III.B further the modifications to PV to accommodate low altitude UAS traffic within restricted airspace.

A. Path Prediction

The probabilistic distribution of UAS positions at the end of each time steps is evaluated using Monte-Carlo simulations, which generates a large number randomized samples within the constrains of the flight capability of the UAS. The 2D simulations presented by Wang et. al. [17] were generated using the simple kinematic equation of motion (Eq. 1).

$$\boldsymbol{a} = \frac{d\boldsymbol{V}}{dt} = \frac{(\boldsymbol{T_{max}} - m\boldsymbol{g} - K_d\boldsymbol{V^2})}{m} \tag{1}$$

where m is the mass of the UAS, $\boldsymbol{a}$ the acceleration vector, $\boldsymbol{T}$ the thrust vector, K_d the empirical drag constant, and $\boldsymbol{V}$ the velocity vector. For the 2D simulations, the UAS was assumed to be at a constant altitude, thus the vertical component of the thrust vector is a constant; furthermore, the K_d of the UAS was assumed to be constant regardless of the attitude of the UAS. The thrust vector for each sample UAS at each time-step were generated using a Gaussian random number generator, which used the value from the previous time-step as mean with a variance of 0.04, or 4% of the maximum thrust available to the UAS. The sum of the final position of all samples is then used to generate the probability of collision.

The assumptions that were used for 2D track generation would no longer be valid for the 3D cases. In particular, since much greater attitude change would be required to achieve a change in altitude, the drag constant would no longer be a single value, but split into the axial and radial component (assuming the UAS as axis-symmetric). After accounting for the change in UAS attitude, the 3D thrust vector would no longer be co-linear with the velocity vector, thus would need to be evaluated as a whole system instead of by individual components. As the vertical motion would be under the influence of gravity, applying the thrust based on normal distributed random number would result in a skewed trajectory that favors the downward motion. Thus, an additional variable ϕ is introduced to describe the elevation angle of the UAS trajectory.

Similar to the previous study, the performance specification of the DJI Inspire 2 was used (Table 1. The UAS model was selected for its weight class (< 7kg), which does not required to have operator license or prior approval to fly [4].

Table 1 Performance specifications of DJI Inspire 2, from Ref. [18]

Variable	Value
UAS Mass (m)	3.4 kg
Maximum Horizontal Speed (S-mode)	26 m/s
Maximum Tilt Angle (S-mode)	40 degree
Maximum Horizontal Speed (P-mode)	22 m/s
Maximum Tilt Angle (P-mode)	25 degree
Maximum Ascend Speed	6 m/s
Maximum Descend Speed	9 m/s

The empirical drag constant for the axial (K_{da}) and radial (K_{dr}) components could then be evaluated using the relationships

$$\begin{cases} \boldsymbol{T} \cdot cos(\omega) = M\boldsymbol{g} \\ \boldsymbol{T} \cdot sin(\omega) = K_d \cdot \boldsymbol{V}^2 \end{cases} \tag{2}$$

and

$$K_d \boldsymbol{V}^2 = K_{da}(\boldsymbol{V} sin(\omega))^2 + K_{dr}(\boldsymbol{V} cos(\omega))^2 \tag{3}$$

we can obtain the linear system of equations for the drag constants:

$$\begin{bmatrix} sin^2(\omega_a) & cos^2(\omega_a) \\ sin^2(\omega_b) & cos^2(\omega_b) \end{bmatrix} \begin{bmatrix} K_{da} \\ K_{dr} \end{bmatrix} = M \cdot \boldsymbol{g} \begin{bmatrix} tan(\omega_a)/\boldsymbol{V_a^2} \\ tan(\omega_b)/\boldsymbol{V_b^2} \end{bmatrix} \tag{4}$$

Using the mass of the DJI Inspire 2 (3.4kg) and the maximum speed with the associated tilt angle, the linear system of equation could be solved to obtain the values of 0.064584 for K_{da} and 0.025079 for K_{dr}.

The equation of motion describing 3D motions of the UAS is the same as the basic form for 2D motion. However, in the case of 3D motion, the acceleration vector and the velocity vector is no longer aligned, while the vertical component of the thrust vector could no longer be solved simply by equating it with the weight of the UAS. Due to its flight dynamics, the direction of Thrust is aligned with the attitude of the UAS (described with vector $\hat{u}$); this allowed the thrust components to be described using the tilt angels (ω_1,ω_2) of the UAS, where ω_1 is the rotation angle about the x-axis and ω_2 about the y-axis of the global frame, where the initial direction of travel is in the y-direction. $\hat{u}$ could then be written as:

$$\hat{\boldsymbol{u}} = \begin{bmatrix} cos(\omega_1)sin(\omega_2) \\ -sin(\omega_1) \\ cos(\omega_1)cos(\omega_2) \end{bmatrix} \tag{5}$$

The evaluation of the drag would be more complicated, since the drag constant would have to be evaluated while accounting for the difference in the direction of motion (velocity vector) and the attitude of the UAS. The velocity vector,

based on the pitch (ϕ) and yaw (θ) angles of the intended travel of the UAS, which is randomly generated at the start of each time step, could be written as:

$$\hat{\boldsymbol{v}} = \begin{bmatrix} sin\theta cos\phi \\ cos\theta cos\phi \\ sin\phi \end{bmatrix} \tag{6}$$

and the drag vector could be written as:

$$\boldsymbol{D} = -\hat{v}[K_{da}(\boldsymbol{V} \cdot \hat{u})^2 + K_{dr}(\boldsymbol{V} \cdot (\hat{v} - (\hat{v} \cdot \hat{u})))^2] \tag{7}$$

The equation of motion could then be solved iteratively using bi-sectional method with the limit:

$$0 < cos\omega_1 cos\omega_2 < cos40^\circ \tag{8}$$

to find the value of ω that would result in $\boldsymbol{T}/|\boldsymbol{T}| = \hat{u}$.

B. Collision Prediction

The collision box used in the 2D collision prediction code is adapted from the Traffic Collision Avoidance System (TCAS) definition [6], using the Distance Modification (DMOD) distance for < 1000 ft Above Ground Level (AGL) as the inner most protected volume. Any UAS, represented by a point source, that entered into that protected volume would be deemed to have collided with the plane. Given that the height of the TCAS protected volume is 850 ft above and below, it would leave less than 150 ft AGL of vertical space for UAS to operate in at the restricted airspace boundary. Thus, collision prediction and risk assessment based on the TCAS protected volume would not be useful in risk evaluation for UAS operating in close proximity to the airport.

The proposed modified protected volume to be used for the 3D case would be based on the Collision Slab from Reich Model that was used by ICAO to evaluate the hazard of intersecting flight corridors [19] (Figs. 1(a)) and the Protected Zone from Metz et al. [16] (Figs. 1(b)) to evaluate the risk of bird strike. The former consisted of a rectangular box with length, width, and height based on the length, wingspan, and the height (without landing gear) of the aircraft; the later consisted of a partial cylinder with the radius of half-wingspan and the diameter of the fuselage as height, but with the volume behind the wing excluded. While differ in shape, the dimensions used in the creation of the "collision boxes," with the exception of height, are mostly the same for similar aircraft class. This is because "the consequence of bird (or UAS) strike on the vertical stabilizer is not as sever as a collision by another aircraft" [16].

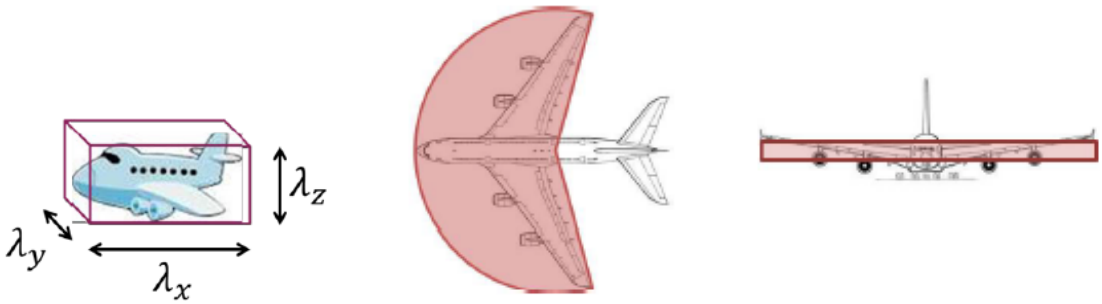

(a) Reich Collision Box (b) Protected Zone for Bird-strike

Fig. 1 (a) Collision box used in the Reich collision risk assessment (from Ref. [19]) and (b) the Protected Zone used by Metz et al. (from Ref. [16]) for collision assessment.

In the Reich collision model, a collision is predicted when the collision slab of the two aircraft intersects; alternatively, when the center of gravity (C.G.) of the intruder aircraft falls within a box of 2λ around the C.G. of the host-aircraft. For collision between an airliner and a UAS, the "collision box" would be the size of $\lambda_{aircraft} + \lambda_{UAS}$, where $\lambda_{aircraft}$

values are based on the weight-averaged aircraft dimensions. Similar modification could be made to the Metz et al. model so the UAS could be treated as a point source.

Additionally, the reported C.G. position of the aircraft is affected by the accuracy of the hardware. For example, early TCAS system favors vertical maneuver instead of lateral ones due to the lack of lateral resolution reported by the TCAS transponder [6]. The uncertainties in the reported aircraft altitude was also a factor during the development of vertical component for the TCAS protected volume [20], where the acceptable altimeter error was stated as 250 ft above 10,000 ft Above Mean Sea Level (AMSL) and 150 ft (45.72 m) below. This is despite the fact that earlier study had shown that the estimated standard deviation in total altimetry system for Air Data Computer (ADC) equipped system at < 5000 ft AMSL is 38 ft (12m) [21]. In a more modern, ADS-B equipped, aircraft with Navigation Accuracy Category for Position (NACp) =8, the reported position would have an estimated position uncertainty (EPU) of less than 0.05 nautical miles (93 m) with no value stated for the estimated position uncertainty (VEPU); for NACp=9 the EPU is less than 30 m and VEPU is less than 45 m [22].

Based on 14 CFR §91.227 [23] published by FAA, the (NACp) of greater or equal to 8 is required for ADS-B equipped aircraft, thus the horizontal uncertainty value of 93 m and vertical uncertainty value of 46 m would be added to the "collision box." That is to say, a cylindrical collision box would have a radius that is the sum of half-wingspan and half- EPU surrounding the reported C.G. position, while the height of the cylinder would be constructed with the sum of half-height of the fuselage and half- VEPU above and below the reported C.G. If a partial cylinder collision box is used, the partial cylinder would be created first before applying the offsets of EPU and VEPU.

Due to the use of Instrument Landing System (ILS) glide slope for landing operation, the reported arrival tracks within the restricted airspace has been shown to have small (< 30 ft) horizontal and vertical deviation [24, 25]. However, little information in available on deviation in departure track, as the Radio Navigation (RNAV) departure chart only specifies the minimum climb slope and minimum height at each waypoint. Additionally, the two airports that was the most studied regarding their departure tracks, Atlanta Airport and Dallas-Fort Worth Airport, both have diverging departure tracks in addition to the runway headings; the data are also presented for the entire Terminal Radar Approach Control (TRACON) area, without detailed information on the track deviation for the segment inside the restricted airspace [26–28]. Several of the departure tracks also involved turning within the restricted airspace, which could lead to variation in lateral position by up to 1 nautical mile due to difference in aircraft performance [27].

For the purpose of this study, the standard ILS 3.5° glide slope will be used for the landing aircraft; for takeoff operations, the minimum climb gradient for each runway would be used while following the runway heading. All arrival tracks were assumed to reach ground at 300 m from the runway threshold (where the ILS beacon is located at), while the departure track would assume the aircraft is airborne at 3200 m from the aft- runway threshold.

The collision prediction code utilizes the intended track of the corresponding operation for the placement of aircraft C.G. at each time step, using a speed of 140 knots for landing and 155 knots for take-off operations. The deviation of the aircraft from the track would be assumed to have contributed to the EPU/VEPU, thus no additional change would be made to the collision box.

IV. Simulation Results and Discussion

Simulations were performed for two scenarios: the first is the 3D collision assessment that would lead to the establishment of Alert Zone boundary for non-cooperative UAS intrusion into the restricted airspace; the second is the assessment of UAS deviation under selected conditions to obtain the respective flight-path buffer required for UAS operation within restricted airspace.

A. Non-Cooperative UAS: Three Dimension Alert Zones For Landing Aircraft

The collision risk assessment for the non-cooperative UAS incursion were conducted using the Monte-Carlo model described in Sec. III.A with the assumption of worst-case intention of intruding into the flight corridor. The intersecting course for the UAS is achieved by re-evaluating the $\bar{\theta}$ and $\bar{\phi}$ for each Monte-Carlo sample at the beginning of every time step so that these two values are always pointing in the direction of the flight corridor. As the UAS moves closer to the waypoint, the maximum velocity for the UAS would decrease to stay within its maximum vertical and horizontal speed limit; this would effectively slow down the UAS to a hover close to the waypoint coordinate. The implementation of the waypoint system significantly reduced the number of simulations needed to create the Alert Zones and prevent the formation of gaps in Alert Zones shown in the previous study [17]. An example of the Monte-Carlo samples distribution with and without a prescribed waypoint is shown in Fig. 2.

The waypoint system would also effectively reduce the spread among the samples as they approach the waypoint.

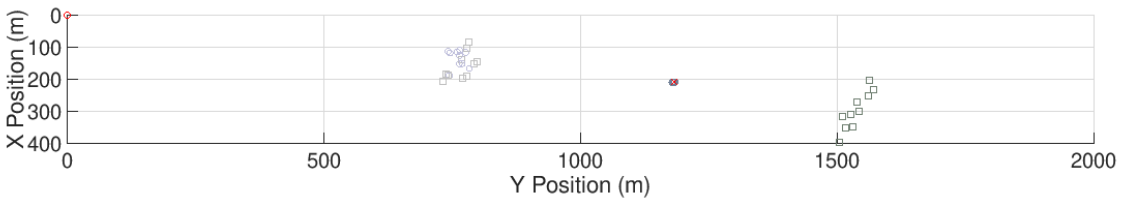

Fig. 2 Sample distributions at t = 50s (light gray) and t = 100s (dark gray) for simulations with (circle) and without (square) a target waypoint set at 010° and 1200 meters from the origin.

This could be beneficial for 3D collision simulations that cover a longer time period, since the vertical spread of 50% of the samples could exceed the vertical component of the protected volume. To simulate the worst-case intention for a landing operation, the target waypoint for the UAS was set to the point on the centerline of the ILS glide path that has the shortest horizontal distance to the initial UAS position.

A test simulation with the 3D collision risk assessment code is presented in Fig. 3 for an aircraft performing landing operation along runway 02C; the position of the UAS at t = 0s, when the aircraft enters the 5 km restricted airspace, is at (-1500,-5000) with an elevation of 200 m above ground level (AGL). The worst-case intention is used to perform this simulation, which set the UAS on a collision course to the flight corridor. The risk assessment is performed every 2 seconds using the position of the Monte-Carlo samples and the protected volume of the aircraft based on a constant landing speed. To compensate for the length of the assessment interval, the protected volume is stretched in the aircraft direction of travel by the aircraft travel distance over the same length of time. Both the protected volumes based on ACAS II (used in the 2D simulations from Ref. [17]) and that from the current study (as described in Sec. III.B) are projected on the ground for size comparison.

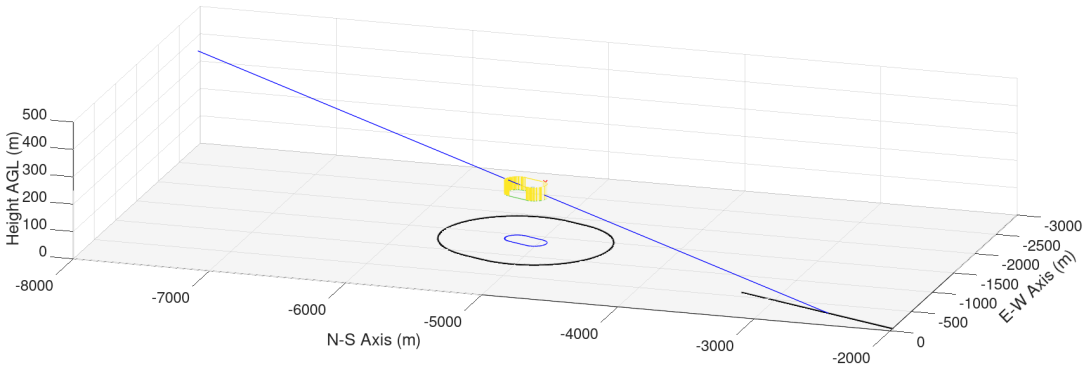

Fig. 3 Isometric view of the runway, protected volumes of the aircraft, the initial position of the UAS, and the distribution of the Monte-Carlo samples at t = 32s with 100% of the samples inside the collision box.

The simulation results showed that more than 50% of the Monte-Carlo samples intrudes into the protected volume of the aircraft by t = 32s. This would indicate that an UAS detected at this position at t = 0s could be a hazard to an aircraft descend into the restricted airspace at the same time.

The 3D Alert Zone for specific aircraft operations would be created by performing the collision simulation for a range of UAS initial positions. These initial positions were created following a 3D grid pattern with uniform spacing of 200m in the horizontal directions and 100m in the vertical direction. The grid is then rotated so the horizontal grids follows the direction of the runway before the entire grid is tilted to match the desired glide slope or climb slope. The grid points that ended up below the ground level ($z < 0$m) are discarded. Fig. 4 shows the initial positions for which > 50% of the Monte-Carlo samples, modeled with the UAS performance data from Table 1, intrudes into the protected volume of a narrowbody passenger aircraft performing a landing operation. The markers are colored to reflect the time when such intrusion occurred. The solid blue line marks the boundary for the deterministic 2D Alert Zone from our previous study, which is based on the maximum range of the UAS.

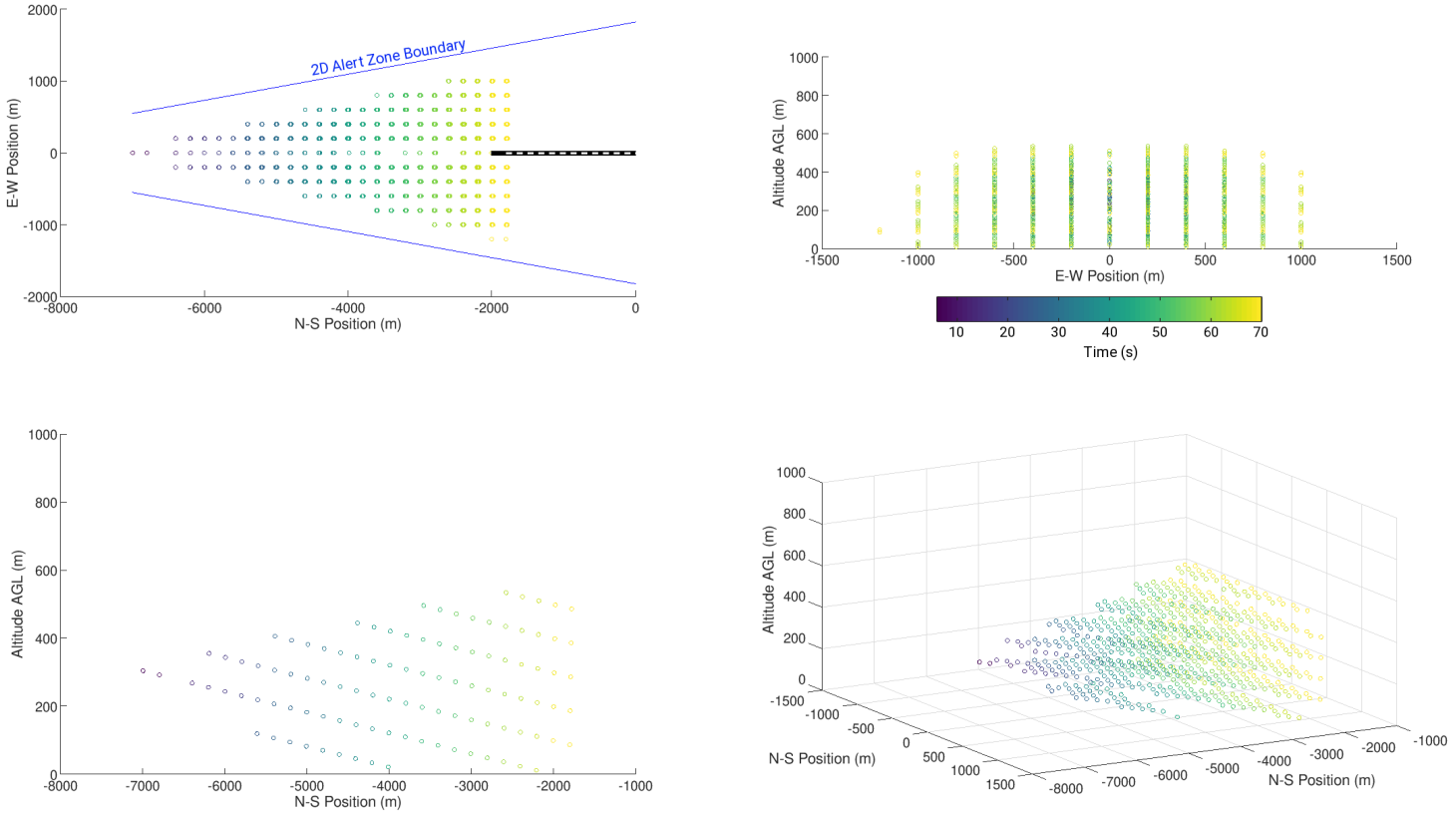

Fig. 4 The 3D alert zone for landing operation of a narrow body commercial jet traveling at 140 knots along a landing glide slope of 3.5°**.**

The new 3D Alert Zone shows that the horizontal extend of the region where UAS initial position falls within is smaller than its 2D counter part. This is likely due to the additional dimension for motion available to the UAS that reduced the likelihood of the UAS taking the most direct path to the flight corridor at maximum speed. An additional factor to consider is the size of the protected volume that was used in the collision prediction: the 2D Alert Zone was generated for a pre-stretched protected volume with a radius of 556m, while the 3D Alert Zone used a radius of 88m. The resulting 3D Alert Zone covers the entire airspace from the glide path to the ground, thus ruling out unmonitored, non-cooperative UAS operation underneath the flight corridor. Instead, cooperative operation of the UAS, where the operator has direct communication with the ATC, would be required.

B. Cooperative UAS Operation in Restricted Airspace with Landing Aircraft

The main difference between cooperative and non-cooperative UAS operation is the availability of two way communication between the ATC and the UAS operators that could aid in resolving possible conflicts. That said, cooperative UAS operation could be anything from a two-way radio for information exchange to automated transponder such as ADS-B. As the previous section has shown that having non-cooperative UAS operating underneath, or in close proximity to, the landing corridor would result in an elevated risk of collision, this section will concentrate on the evaluation of factors influencing the collision risk for cooperative UAS operation in such airspace.

Two hypothetical scenarios will be considered in this study: an operator controlled UAS with no GPS equipped; an operator controlled UAS using ADS-B reported position at NACp=9 for navigation. For the first case, the uncertainty in UAS position was assumed to be the same as that used in Section IV.A, with the ϕ and θ randomly distributed with the variance $\sigma^2 = 4\%$ of the maximum value. The variance for the random distribution is retained in the second case, with the exception that the standard deviation of the UAS samples is checked against the EPU every 3 seconds, which is the maximum allowed update interval for ADS-B [5]; in the event that the boundary that contains 95% of the samples (2σ) exceed the EPU, the UAS will be assumed to be re-positioned to the "true" position along the track by the next update time. Figures 5 and 6 shows the default distribution of the Monte-Carlo samples using $\sigma^2 = 4\%$ of the maximum value for the randomized normal distribution.

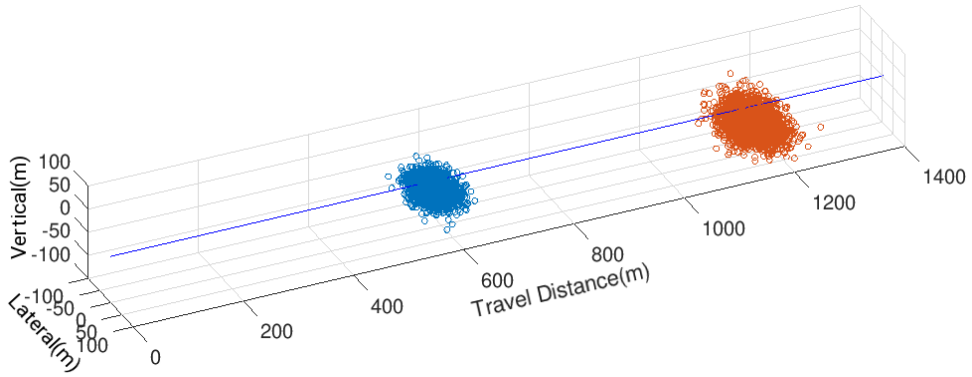

Fig. 5 Default distribution of UAS for $t = 35$s and $t = 70$s. The 2000 samples at$t = 35$ have $\bar{x} = -0.11$m and $\sigma = 28.50$m; $t = 70$ have $\bar{x} = 0.57$m and $\sigma = 40.13$m.

One of the issue observed in Fig. 6 was the downward bias in the resulting distribution despite the prescribed heading with $\bar{\phi} = 0$ and $\bar{\theta} = 0$. This is due to the difference in maximum ascend and descend speed of the UAS, as shown in Table 1; the UAS could travel a longer vertical distance per time step descending than ascending given the same $|\phi|$. The end result is approximately $-1.75°$ in mean inclination from the targeted direction, or around 30.5m drop for every kilometer traveled. Additionally, the mean travel distance from the initial position in Fig. 6(a) is larger than Fig. 6(b). This is due to the speed limit imposed by the flight controller as specified in Table 1; the relationship between the maximum speed of the UAS and ϕ, as constrained by the speed limit, is shown in Fig. 7.

The lateral and the vertical position distribution of the UAS samples showed that for a flight path of ~ 1 km, the results for the two cases would be identical until $t = 9$s: neither the vertical or horizontal distribution exceed the uncertainty range for ADS-B with NACp = 9 until then. By $t = 12$s, the simulated UAS samples would results in $\bar{x} = 0.061$m, $\sigma_x = 15.162$m and $\bar{z} = -5.372$m, $\sigma_z = 7.023$m, at which point the horizontal heading correction would be applied. The simulation showed that the UAS could have traveled for approximately 200m before the deviation from

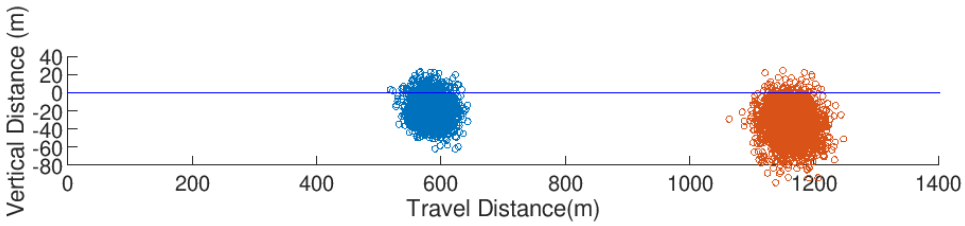

(a) Manufacturer Specification (6/9 m/s for Ascend/Descend)

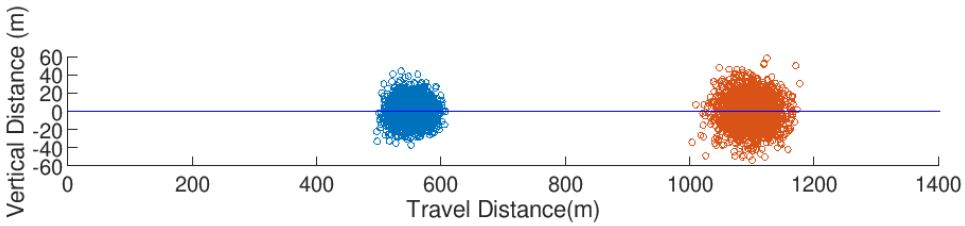

(b) Equal Max. Ascend/Descend Speed (6 m/s)

Fig. 6 Effect of unequal ascend and descend speed limit on vertical distribution of UAS for $t = 35$s and $t = 70$s. The 2000 samples at $t = 70$ have (a) $\bar{z} = -35.48$m and $\sigma = 18.55$m, and (b) $\bar{z} = -0.41$m and $\sigma = 16.43$m.

the assigned track could be corrected. As for the vertical deviation, the Monte-Carlo samples showed that it would take over 50s for the $2\sigma_z$ to exceed the VEPU, at which point the UAS would have traveled over 750m.

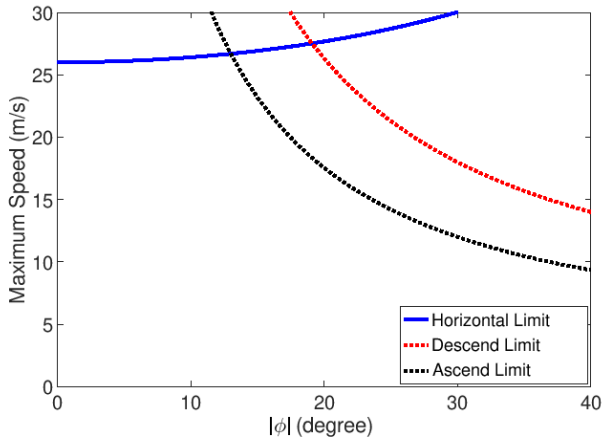

Fig. 7 The maximum speed attainable by the UAS based on the manufacturer specified maximum horizontal, ascending, and descending speed limits.

Based on the simulation results, the expected flight corridor for the UAV controlled with ADS-B out (case 2) would eventually grow into an elliptical cylinder with the horizontal axis of ~ 30.4m and the vertical axis of approximately 24m with around 1.75° downward slope. This would be functionally identical to a cylinder with EPU for horizontal axis and VEPU as vertical axis for very long travel distances, but the size of the airspace needed could be less for shorter hops. Assuming that the landing aircraft could deviate by $\sigma_z = 30$ft(10m) from the centerline of the glide slope, the UAS track would need a vertical separation distance of at least 40m (3-σ) below the glide slope centerline to operate. Assuming a vertical buffer of 20m above ground is desired for the UAS track, the cooperative UAS could operate insider the restricted airspace on the landing side as long as the track is ≥ 680m away from the runway threshold. Environmental factors such as wind conditions and wake turbulence could further increase the separation needed.

V. Conclusion and Future Work

3D UAS movement model was created for Monte-Carlo simulation that estimates the collision risk posed by non-cooperative UAS, modeled after the flight characteristics of the DJI Inspire 2, intruding into the terminal restricted airspace. The simulations were conducted within the 5km terminal airspace using UAS initial positions uniformly spaced at 200m horizontal intervals and 100m vertical interval. A initial position is marked as hazardous if $\geq 50\%$ of the samples that originated there intrudes into the protected volume of the aircraft, assuming the UAS is traveling with the worst-case intention. These initial positions would form the 3D Alert Zone for the conflict UAS-aircraft pair, within which the UAS sighting should lead to the abortion of aircraft operation and the closure of the airport. Note that the 3D Alert Zone boundary is different depending on the UAS-aircraft pairing. The 3D Alert Zone for a UAS modeled after the DJI Inspire 2 and a landing narrowbody passenger aircraft is presented in this paper. Future work would be done on performing the same analysis for the take-off cases with different minimum climb slope requirements, as well as on different conflict pair.

The 3D UAS movement model were also used to analyze the spread in UAS track as it travels along a prescribed path. Simulations were conducted to emulate the UAS tracks controlled by a pilot, the first case assuming that the pilot in controlling by sight, while the second case assume that the pilot is assisted by the ADS-B Out broadcasted by the UAS at NACp=9. The UAS were assumed to be traveling with a random spread at $\sigma^2 = 20\%$ of maximum value for ϕ and θ. Without heading correction the standard deviation of the UAS samples would reach $\sigma_x = 26.15$ by $t = 70$s, while navigating with ADS-B would limit the deviation to $\sigma_x = 15$m throughout. This suggests that UAS operation under the flight corridor could be feasible given that the UAS is equipped with navigational aid and the distance between the UAS track and the flight path exceed the deviation of the UAS and aircraft tracks. The deviation from UAS track could be further reduced by limiting the random spread, increasing the broadcast frequency of the transponder, or by shifting the short-term navigation task to the onboard controller.

Overall, the 3D UAS movement model has been demonstrated to be useful in collision assessment in a variety of scenarios. More work is needed to determine the Alert Zones within the aerodrome for aircraft taking off with different minimum climb rate requirement, and the implication of these Alert Zones on the UAS collision mitigation strategy of the airport operator as well as the installation requirements for UAS detection equipment. Additionally, further research is required to better quantify the expected deviation of UAS over time under direct human control as well as the possible factors, and quantify their effects, influencing the deviation of UAS from its assigned track.

Acknowledgment

We would like to thank Air Traffic Management Research Institute for funding this research under Programme 2: Urban Aerial Transport Traffic Management & Systems.

References

[1] Deulgaonkar, P., "Shutting down Dubai International Airport due to a drone costs $100,000 a minute," *Arabian Business*, 09 Jul 2017. URL `http://www.arabianbusiness.com/content/375851-drone-costs-100000-minute-loss-to-uae-airports`.

[2] Corporation, B. B., "Drone causes Gatwick Airport disruption," *BBC*, 03 July 2017. URL `http://www.bbc.com/news/uk-40476264`.

[3] George, T., "Video shows drone coming close to plane landing at McCarran," *KTNV*, 04 Feb, 2018. URL `https://www.ktnv.com/news/video-shows-drone-coming-close-to-plane-landing-at-mccarran`.

[4] *Air Navigation Order*, Civil Aviation Authority of Singapore, September, 2018. PART XA: Unmanned Aircraft Operations and Activities.

[5] *Automatic Dependent Surveillance-Broadcast (ADS-B) Flight Inspection*, Federal Aviation Administration, Washington D.C., U.S.A, 2014.

[6] EUROCONTROL (ed.), *ACAS Guide: Airborne Collision Avoidance Systems (incorporating TCAS II versions 7.0 & 7.1 and introduction to ACAS X)*, 2nd ed., European Organisation for the Safety of Air Navigation, Brussels, Belgium, 2016.

[7] Looze, D., Plotnikov, M., and Wicks, R., "Current Counter-Drone Technology Solutions to Shield Airports and Approach and Departure Corridors," Tech. rep., Massachusetts Department of Transportation, Boston, MA, U.S.A., December 2016.

[8] Angelov, P. (ed.), *Sense and Avoid in UAS: Research and Applications*, John Wiley & Sons., Hoboken, NJ, U.S.A., 2012.

[9] Kim, K.-Y., Park, J.-W., and Tahk, M.-J., "UAV collision avoidance using probabilistic method in 3-D," *2007 International Conference on Control, Automation and Systems*, 2007, pp. 826–829. doi:10.1109/ICCAS.2007.4407015.

[10] Krozel, J., Peters, M. E., and Hunter, G., "Conflict Detection and Resolution for Future Air Transport Management," Tech. Rep. NASA-CR-97-295944, NASA Ames Research Center, Moffett Field, CA, U.S.A., 1997.

[11] Kuchar, J. K., and Yang, L. C., "A Review of Conflict Detection and Resolution Modeling Methods," *IEEE Transaction on Intelligent Transportation Systems*, Vol. 1, No. 4, 2000, pp. 179–189.

[12] Paielli, R. A., and Erzberger, H., "Conflict Probability Estimation for Free Flight," *Journal of Guidance, Control, and Dynamics*, Vol. 20, No. 3, 1997, pp. 588–596.

[13] Taylor, D. H., "Uncertainty in Collision Avoidance Maneuvering," *Journal of Navigation*, Vol. 43, No. 2, 1990, pp. 238–245.

[14] Carpenter, B. D., and Kuchar, J. K., "Probability Based Collision Alerting Logic for Closely-Spaced Parallel Approach," *35th Aerospace Sciences Meeting and Exhibit*, American Institute of Aeronautics and Astronautics, Reno, NV, U.S.A., 1997. AIAA-97-0222.

[15] Yang, L. C., and Kuchar, J. K., "Using Intent Information in Probabilistic Conflict Analysis," *Guidance, Navigation, and Control Conference and Exhibit*, American Institute of Aeronautics and Astronautics, Boston, MA, U.S.A., 1998. AIAA-98-4237.

[16] Metz, I. C., Ellerbroek, J., Mühlhausen, T., Kügler, D., and Hoekstra, J. M., "Simulating the Risk of Bird Strike," *Seventh SESAR Innovation Days*, 2017.

[17] Wang, C. J., Tan, S. K., Ting, L. K. J., and Low, K. H., "Impact of Sensors on Collision Risk Prediction for Non-Cooperative Traffic in Terminal Airspace," *International Conference for Unmanned Aircraft Systems*, 2018.

[18] DJI Technology Co., Ltd, *Inspire 2 User Manual*, 1st ed., SZ DJI Technology Co., Ltd, Shenzhen, China, 2017.

[19] Civil, J., and Daly, H., "The Longitudinal Reich Collision Risk Model," *Separation And Airspace Safety Panel (SASP) Meeting Of The Working Group Of The Whole*, 2012.

[20] Bagnall, J. J., and Kay, I. W., "Review and Analysis of Some Collision Avoidance Algorithms with Particular Reference to ANTC-117," Tech. Rep. FAA-RD-75-72, Federal Aviation Administration, Washington D.C., U.S.A., 1975.

[21] Lebron, Z. A. S. N. A. J., J.E., and Harman, W., "System safety study of minimum TCAS II (Traffic Alert and Collision Avoidance System)," Tech. Rep. DOT/FAA/PM-83/36, 1983.

[22] *Technical Provisions for Mode S Services and Extended Squitter*, 2nd ed., International Civil Aviation Organization, 2017. Amendment 1.

[23] *Automatic Dependent Surveillance-Broadcast (Ads-B) Out Equipment Performance Requirements*, 14 CFR §91.227, Federal Aviation Administration, 2014.

[24] Hall, T., and Soares, M., "Analysis of localizer and glide slope Flight Technical Error," *2008 IEEE/AIAA 27th Digital Avionics Systems Conference*, 2008, pp. 2.D.2–1–2.D.2–9. doi:10.1109/DASC.2008.4702786.

[25] Zhang, Y., Shortle, J., and Sherry, L., "Comparison of arrival tracks at different airports," *4th International Conference on Research in Air Transportation*, 2010, pp. 481–486.

[26] Sprong, K., McCrabb, R., and Mayer, R., "Evaluation of RNAV Departure Operations at Atlanta Hartsfield-Jackson International Airport," *6th AIAA Aviation Technology, Integration and Operations Conference (ATIO)*, 2006. AIAA-2006-7772.

[27] Borchers, P. F., and Day, K., "Analysis of divergences from area navigation departure routes at DFW airport," *2009 IEEE/AIAA 28th Digital Avionics Systems Conference*, 2009, pp. 3.A.1–1–3.A.1–16. doi:10.1109/DASC.2009.5347532.

[28] Roach, K., and Robinson, J., "A terminal area analysis of continuous ascent departure fuel use at Dallas/Fort Worth international airport," *10th AIAA Aviation Technology, Integration, and Operations (ATIO) Conference*, 2010. AIAA-2010-9379.